Synthesis of Aero-Propulsive Interaction Studies Applied to Conceptual Hybrid-Electric Aircraft Design

Hoogreef, Maurice; de Vries, Reynard; Sinnige, Tomas; Vos, Roelof

DOI
10.2514/6.2020-0503

Publication date
2020

Document Version
Final published version

Published in
AIAA Scitech 2020 Forum

AIAA SciTech Forum
6-10 January 2020, Orlando, FL
AIAA Scitech 2020 Forum

10.2514/6.2020-0503

Synthesis of Aero-Propulsive Interaction Studies Applied to Conceptual Hybrid-Electric Aircraft Design

Maurice F. M. Hoogreef*, Reynard de Vries†, Tomas Sinnige‡ and Roelof Vos§
Delft University of Technology, Faculty of Aerospace Engineering, Delft, the Netherlands

This paper presents a synthesis of aero-propulsive interaction studies performed at Delft University of Technology, applied to conceptual aircraft designs with distributed hybrid-electric propulsion (DHEP). The studied aero-propulsive interactions include tip-mounted propulsion, wing leading-edge distributed propulsion and boundary-layer ingestion, combined with different primary propulsion-system arrangements. This paper starts with a description of the applied design framework and an overview of the aero-propulsive interactions. Subsequently, the different aircraft configurations are sized for a set of top-level requirements covering the range between regional turboprop to typical narrow-body turbofan aircraft. Results indicate that lower shaft power ratios show better performance, with the unoptimized DHEP concepts showing values of maximum take-off mass (MTOM) and payload-range energy efficiency (PREE) comparable to their reference aircraft. It was shown that beyond 20% shaft power ratio, the PREE decreases and MTOM increases much more than between 10% and 20%, indicating a possible local optimum between these values since even lower values did not yield any significant improvements. The benefits of tip-mounted propulsion are found to be constrained by the propeller blade tip Mach number in this particular analysis for the selected reference blade loading distribution. At the high range case for Mach 0.5, it can be seen that the distributed propulsion systems show the largest improvement.

Nomenclature

Latin Symbols

AR	=	Aspect ratio (∼)
A	=	Cable cross-sectional area (m^2)
C_D	=	Drag coefficient (∼)
C_L	=	Lift coefficient (∼)
C_{L_α}	=	Lift curve slope (Rad^{-1})
I	=	Current (A)
J	=	Advance Ratio (∼)
M	=	Mach number (∼)
P	=	Power (W)
T	=	Thrust (N)
TC	=	Thrust Coefficient $\frac{T}{\rho \cdot V_{inf}{}^2 \cdot d^2}$ (∼)
S	=	Wing area (m^2)
V	=	Velocity (m/s)
W	=	Weight (N)
b	=	Span (m)
d	=	Diameter (m)
l	=	Length (m)
m	=	Mass (kg)

Greek Symbols

α	=	Wing angle of attack (deg)
α_p	=	Propeller incidence angle (deg)
η_p	=	Propulsive efficiency (∼)
Λ	=	Sweep angle (deg)
λ	=	Taper ratio (∼)
ξ	=	Gas turbine throttle (∼)
ψ	=	Supplied power ratio (∼)
φ	=	Shaft power ratio (∼)

Acronyms

BC	=	Business class
BLI	=	Boundary layer ingestion
CG	=	Center of gravity
DHEP	=	Distributed hybrid electric propulsion
DOC	=	Direct operating cost
ESP	=	Equivalent specific power
FEM	=	Finite element method
FL	=	Flight Level
FMDP	=	Fuselage-mounted ducted propeller
HEP	=	Hybrid electric propulsion

*Assistant Professor, Flight Performance and Propulsion, Kluyverweg 1, 2629HS Delft, m.f.m.hoogreef@tudelft.nl, AIAA Member
†PhD candidate, Flight Performance and Propulsion, Kluyverweg 1, 2629HS Delft, AIAA Member
‡Assistant Professor, Flight Performance and Propulsion, Kluyverweg 1, 2629HS Delft, AIAA Member
§Assistant Professor, Flight Performance and Propulsion, Kluyverweg 1, 2629HS Delft, AIAA Associate Fellow

HTMP	=	Horizontal tail mounted propeller	OEI	=	One engine inoperative
ICA	=	Initial cruise altitude	OEM	=	Operational empty mass
ISA	=	International standard atmosphere	SL	=	Sea-level
KCAS	=	Knots calibrated airspeed	T/O	=	Take-off
KPI	=	Key performance indicator	PIV	=	Particle image velocimetry
LE	=	leading-edge	PREE	=	Payload range energy efficiency
			TLAR	=	Top level aircraft requirement
LLM	=	Lifting-line model	WI	=	Wake ingestion
LPA	=	Large passenger aircraft	WMP	=	Wing-mounted propeller
MLM	=	Maximum landing mass	TOFL	=	Take-off field length
MTOM	=	Maximum take-off mass	TT	=	Time to climb
NASA	=	National Aeronautics and Space Administration	YC	=	Economy class

I. Introduction

Modern day aviation's climate impact is one of the key focus areas of research efforts in pursuit of, for example, the goals identified by the Air Transport Action Group* or the European Commission in its Flightpath 2050 [1] vision on aviation. Significant research is being performed in the area of distributed propulsion and hybrid-electric propulsion, aimed at exploiting their potential synergistic benefits (e.g. [2–15]). The versatility offered by electrical systems allows distribution of powertrain components along the airframe, potentially resulting in beneficial aero-propulsive interactions. The latter is important, as these must outweigh any mass penalties introduced by electrification of the powertrains.

Over the past years, significant effort has been spent at Delft University of Technology to experimentally and computationally assess the performance of highly integrated propulsion systems. Among these are leading-edge [16, 17] and over-the-wing distributed propulsion systems[16, 18], tip-mounted propellers [19, 20], tail-mounted propellers [21–23] and Boundary Layer Ingestion (BLI) or wake-filling of aft-mounted propulsors [24, 25]. However, so far models derived from subsystem studies of aero-propulsive interaction effects have only been coupled to the conceptual design of aircraft to a limited extent (e.g. [4, 13, 14, 26]), but no systematic study has been performed comparing the different distributed-propulsion architectures. Especially for distributed propulsion, these effects can have a large impact on the design points (i.e. wing loading, power loading, mass, etc.). Therefore, a new generic sizing method for DHEP aircraft that includes these effects was developed by de Vries et al. [27] The original sizing method focused on leading-edge and over-the-wing propulsion; this article presents an extension of this sizing method to the aforementioned aero-propulsive interaction studies. This development has been performed under the umbrella of the EU project NOVAIR. NOVAIR is part of work package 1.6.1.4 of the Clean Sky 2 program targeting Large Passenger Aircraft (LPA). The goal of NOVAIR is to investigate what synergistic effects between the propulsion system and airframe can be exploited in future aircraft and what their impact is on key performance metrics such as overall energy consumption and mass.

This paper presents the preliminary findings for conceptual hybrid-electric propulsion (HEP) aircraft designs, fitted with a partial turbo-electric powertrain, evaluated for a set of top-level aircraft requirements (TLAR), variable technology scenarios and different shaft power ratios. These include a design payload of 20 metric tons for 150 passengers, a harmonic range of 1100 to 2000 nmi and a cruise Mach number ranging from 0.5 to 0.6. The powertrain architecture and mission requirements are based on the findings of sensitivity studies carried out previously [13, 28]. To this end, the sizing method [27] has been extended and coupled to the in-house developed Aircraft Design Initiator (or simply *Initiator*), a conceptual design tool synthesizing aircraft for given TLARs using a predefined convergence loop [29]. The sizing tool is described in Sec. II, while the aero-propulsive models that were integrated in the tool are briefly discussed in Sec. III. Section IV then presents the results of the reference aircraft, while Sec. V analyzes the results for the different HEP concepts and mission requirements.

II. Aircraft sizing process

The conceptual aircaftdesign of the different aircraft configurations is performed using the "Initiator" design tool. This software tool performs a design convergence over several disciplinary analyses, including handbook methods,

*Air transport action group, Facts & Figures, May 2016, `https://www.atag.org/facts-figures.html`, visited on 7 June 2018

empirical data and physics-based methods. The process flow of the Initiator is shown schematically in Figure 1. The Initiator itself can be used to assess the impact of small and large changes to the aircraft on so-called key performance indicators (KPIs) in the conceptual design of CS-25 aircraft. It supports propeller-powered and turbofan-powered aircraft, as well as conventional tube-and-wing aircraft and (to some degree) blended-wing-body aircraft, three-surface aircraft, and box-wing aircraft. A description of the Initiator can be found in Elmendorp et al. [29]. Furthermore, the Initiator uses a convergence process for the synthesis, in which the design variables are altered iteratively until a predefined set of KPIs converge below a certain threshold. In other words, the Initiator uses a process of design "feasilization" [30], rather than optimization. Therefore, constraints are not exposed to an optimizer and no explicit design variables exist that are under control of an optimizer.

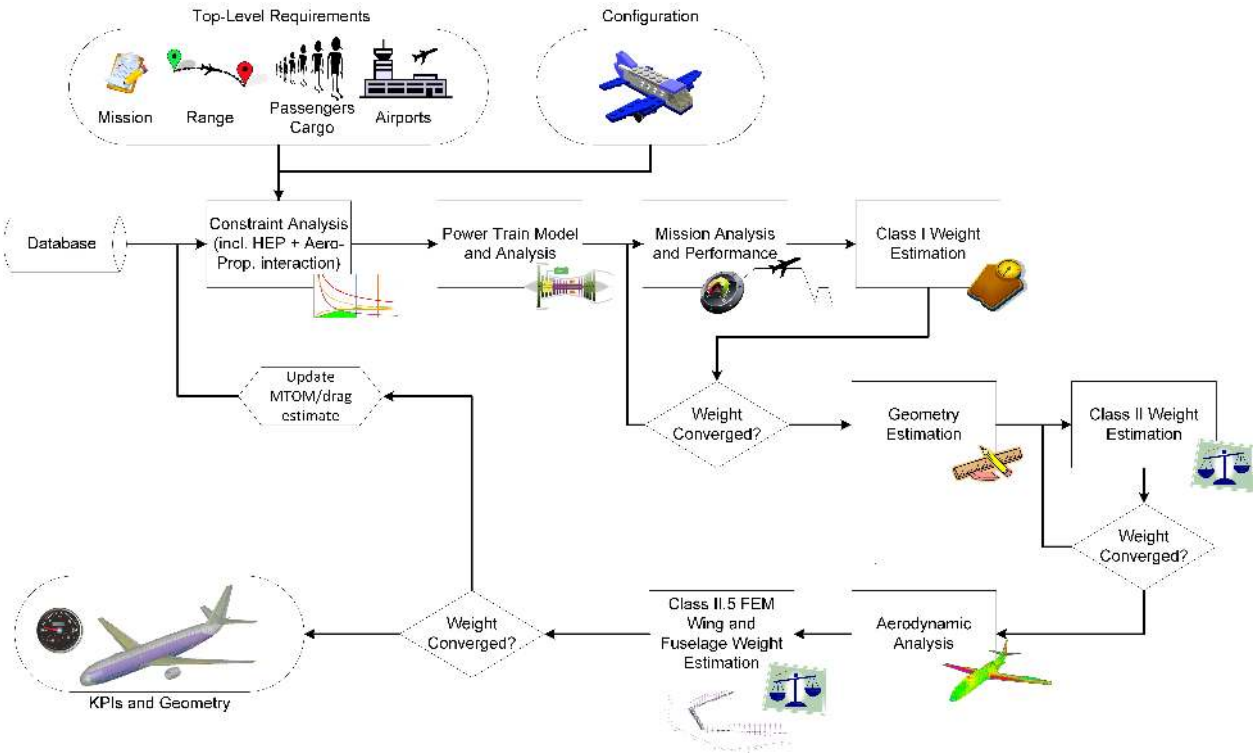

Fig. 1 Illustration of the *Initiator* process flow for the design of DHEP aircraft.

Figure 1 only shows the process flow at an aggregated level; many of the analysis or sizing modules represent different smaller modules. For example, the "Geometry Estimation" contains more than 20 individual modules dimensioning aircraft geometry. Many modules have a dependency on other modules. For example, when only the module "Class-II Weight Estimation" is triggered, it first evaluates all the preceding modules, including the Class-I convergence.

The "Class-II.5 weight estimation" includes a semi-analytical fuselage weight estimation method ([31–33]) and a finite-element (FEM) based wing weight estimation [34] to incorporate the effects of distributed propulsion on wing structure. This includes 2.5G landing loads, 2.5G pull-up at maximum zero fuel weight, as well as a 2.5G pull-up at maximum take-off weight. All wing-mounted masses (engines, generators, fuel tanks, etc.) are considered as either distributed masses or point-masses and are included as loads on the structure.

The convergence loop for the DHEP aircraft design actually consists of multiple convergences; one on Class-I and mission analysis, one on the Class-II weight estimation, one Class-II.5 weight estimation and an overarching loop on the start of the process and the outcomes of the Class-II and Class-II.5 loops. The latter converges on the maximum take-off mass (MTOM). Modifications have been made to the existing Initiator modules to accommodate the sizing of DHEP aircraft, such as mass estimations of electric motors and batteries.

A. Preliminary sizing - wing/power loading diagram

The first convergence loop starts with extracting data from a database of reference aircraft. With this information, an estimate of MTOM is made. In the subsequent module, the required power and wing size are computed based on a user-specified set of top level aircraft requirements (TLARs) in addition to performance requirements stemming from regulations (FAR/CS 25). The sizing methodology that is followed is illustrated graphically in Figure 2; the full description of the Class-I DHEP sizing method can be found in Ref. [27] The hybrid electric preliminary sizing method developed by de Vries et al. [27] has been compared to another sizing approach as developed by Finger et al. [35]; the comparison of both methods in Finger et al. [36] shows good agreement between results.

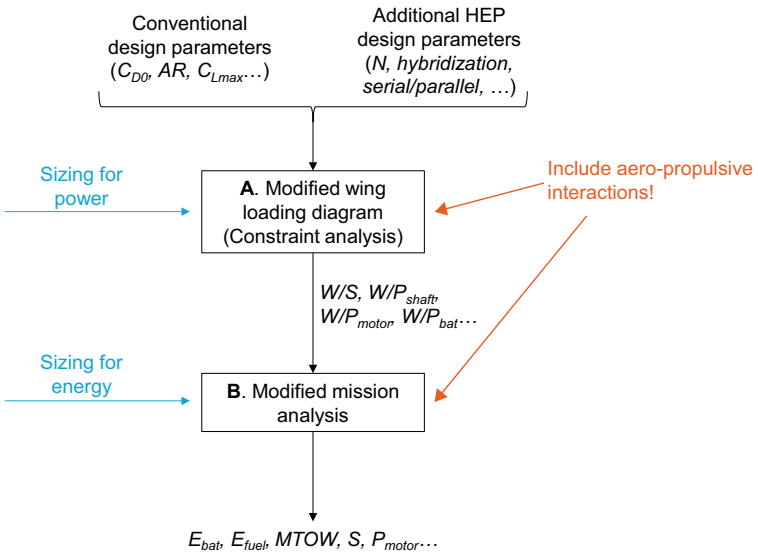

Fig. 2 Schematic flow of conceptual sizing for power and energy.

A key feature of this method is that it considers the aircraft as a point mass, balancing forces and accelerations for each performance requirement. For the representation of the powertrain a simplified model is used, following the six types of layouts proposed by Felder [2] and later adopted by the National Academy of Sciences [37]: conventional, series, parallel, turbo-electric, partial turbo-electric and series/parallel partial hybrid. Additionally, three power controls are included in the model: Gas turbine throttle (ξ), Supplied power ratio (ψ) and Shaft power ratio (φ).

Moreover, the method allows including aero-propulsive effects in the assessment of different constraints in the design-point diagram. Such constraints are, for example, related to take-off and cruise performance or climb performance in one-engine-inoperative scenarios. Normally, these constraints are decoupled from propulsive influences. However, especially for distributed propulsion systems, these effects can be beneficial in terms of wing sizing (if a primary propulsion source provides thrust). As such, lift and drag for equilibrium flight become coupled to thrust:

$$C_{L_{\text{total}}} = C_{L_{\text{isolated}}} + \Delta C_{L_{\text{thrust-induced}}} \tag{1}$$

$$C_{D_{\text{total}}} = C_{D_0} + C_{D_{\text{lift-induced}}} + \Delta C_{D_{\text{thrust-induced}}} \tag{2}$$

These contributions are also included in the drag polar of the aircraft in the mission analysis. Additionally, the subsystems are modeled as separate point-masses in the Class-II and Class-II.5 weight estimations, such that their influences on aircraft MTOM and energy consumption are considered, as well as the impact on the structural wing mass in the FEM weight estimation.

In the present study, the main propulsion system will be coupled to additional propulsion chains including a hybrid-electric powertrain (partial turbo-electric architecture) for the aforementioned cases. The main engine locations are similar to those reported in [26]: conventional wing-mounted propellers (WMP), horizontal-tail-mounted propellers (HTMP) as studied by [21, 22] and fuselage-mounted ducted propellers (FMDP) as studied by [23]. The modeling of the propulsive empennage of the FDMP configuration is reported by Vos and Hoogreef [26]. Stabilizer mounted propellers have also been studied in the Clean Sky 2 project IRON[†].

[†]IRON - Innovative turbopROp configuratioN, Clean Sky 2, IADP Regional, topic: JTI-CS2-CPW02-REG-01-03

B. Mass estimations of components related to hybrid-electric powertrains

This Section explains how the additional components present in a hybrid-electric powertrain are included in the component weight estimation methods.

Electromotors, generators, inverters, power electronics and cooling

The mass estimation of all components of the electrical drivetrain (electromotors, generators, inverters and power electronics) follows the approach of a "combined specific power" based on the specific power (SP) of each component as presented in de Vries et al. [28]. Here a distinction between motors and generators is made in the mass estimation, and an "equivalent specific power" which combines the electrical machine and associated transformer is used:

$$\mathrm{ESP} \approx \sum_{i=1}^{n} \frac{1}{(1/\mathrm{SP}_i)}. \tag{3}$$

This provides a "black box" approach, suitable for conceptual sizing that provides a simplified, top-level understanding of the effects of powertrain technology levels, that is independent of the particular design of the electrical system, as it does not require information regarding every component in the powertrain. Table 1 presents the ESP computed for the three hypothetical technology scenarios. The electrical drivetrain is assumed to consist of electrical machines (generators and motors) and power converters (rectifiers and inverters). An additional 30% mass penalty is added to account for additional power distribution and cooling aspects.

Table 1 ESP for three hypothetical technology scenarios from [28].

Scenario	Electrical machines	Power converters	PMAD/cooling		
	SP [kW/kg]	SP [kW/kg]	weight penalty		ESP [kW/kg]
Near-term	9	13	30%	→	3.7
Mid-term	13	19	30%	→	5.4
Long-term	22	32	30%	→	9.1

The *shaft power ratio* is used to characterize the power share between the primary and secondary propulsion system:

$$\varphi = \frac{P_{s2}}{P_{s1} + P_{s2}}. \tag{4}$$

For the design studies, this share will be varied to study the effects on aircraft level of subtracting more or less power from the turbomachinery, which is used by the distributed electric propulsors. While the aero-propulsive benefit may increase for larger power shares (larger secondary propulsors), their mass penalty will also increase. Therefore, a sweep should indicate when the mass increase becomes the dominating effect.

Cables

To estimate the mass of additional electrical cables required to transmit power between motors and generators, a very rudimentary estimation is made for the distance between all electromotors (on one side of the aircraft) and a generator on the same side of the aircraft. The generator itself is always assumed to be located at the turbine. The distance between the components (i.e. required cable length) is estimated as the sum of the difference between respective x, y and z coordinates:

$$l_{\mathrm{cable}} = \Sigma(|x_{\mathrm{generator}} - x_{\mathrm{motor}}| + |y_{\mathrm{generator}} - y_{\mathrm{motor}}| + |z_{\mathrm{generator}} - z_{\mathrm{motor}}|) \tag{5}$$

This cable length is then summed for all motors on one side and multiplied by two to get the total mass. Every cable is assumed to consist of three wires; hence the total length is multiplied by three. For the BLI fan, it is assumed that a cable runs to both generators. This cable length is split between a component inside the wing and a component inside the fuselage, to be properly accounted as a distributed mass (both for CG and FEM weight estimation). Redundancy is included through a safety factor of two.

The average power over a cable is used to determine the current assuming a 3kV system. The area of copper required is then estimated according to the formula by Stückl [38]:

$$A_{\mathrm{copper}} = 0.0144 \cdot I^{1.4642} \tag{6}$$

To estimate the mass of these electric cables, a regression is made between data available from the reinforced sheathed high temperature, extra flexible power cables FLAMEX SI EN 50382-2 Type FXZăfrom Nexans[‡]. For different cross-sectional areas and a maximum temperature in use of 150deg Celsius, the following data is available:

Table 2 Cable data for FLAMEX SI EN 50382-2 Type FXZ

Area (mm^2)	**Mass** (kg/km)
25	371
35	438
50	579
70	935
95	980
120	1480
150	1505
185	2240

Based on the information from Table 2 a linear regression (with an R^2 of 0.96) can be made, resulting in the following expression for cable mass per kilometer as a function of cross-sectional area in squared millimeter:

$$m_{cable}[kg/km] = 58.196 + 11.044 \cdot A_{cable}[mm^2] \tag{7}$$

III. Aero-propulsive modeling for conceptual aircraft design

The use of novel propulsion systems affects both the aerodynamic performance and the weight estimation of hybrid-electric aircraft. For the preliminary sizing process, the changes in lift, drag, and propulsive efficiency due to aero-propulsive interaction must be estimated and incorporated in the point performance equations of the aircraft, as discussed in the previous section. This section describes how the aero-propulsive effects were computed for conventional tractor propellers, leading-edge distributed propellers, tip-mounted propellers, and boundary-layer-ingesting propellers.

A. Wing-Mounted tractor propellers (conventional, distributed, tip-mounted)

Interactions between tractor-mounted propellers and a wing occur on aircraft with a conventional turboprop layout, but also on configurations with distributed leading-edge propellers for high-lift augmentation, or tip-mounted propellers for induced-drag reduction. The downstream interaction between such tractor propellers and the wing was modeled using a lifting-line model (LLM). In this LLM, the propellers are represented by actuator disks. Realistic disk loading distributions are obtained by scaling a normalized blade loading distribution (thrust and tangential force) from a reference propeller with the known thrust level of the propellers in the present study. The thrust and tangential-force distributions are then used to compute both axial and tangential induced velocities at the position of the lifting line using classic momentum theory. In this process, a slipstream contraction model is used to account for the axial separation between the propeller plane and the wing leading-edge.

The propeller-induced velocities are included as additional induced velocities at the lifting line, thus modifying the wing's circulation distribution. Because of the finite propeller slipstream height, a correction needs to be applied to the local section lift coefficients. For this purpose, the model by Ting [39, 40] was used. The implementation of this correction into the lifting line approach will be explained in more detail in a future publication. With the known section lift distributions and induced angles of attack, the wing lift and induced drag can be computed directly. The slipstream interaction generally increases lift (due to increased dynamic pressure and swirl in the slipstream), and decreases induced drag (due to a swirl-induced forward tilting of the lift vector) in case of inboard-up rotating propellers [16]. Besides modifying lift and induced drag, the propeller slipstream interaction also affects the skin-friction drag of the downstream wing. This was accounted for using an approximate method. The skin-friction coefficient was computed assuming a flat-plate turbulent boundary layer. This coefficient was then converted into a skin-friction drag coefficient using a form factor proposed by Torenbeek [41].

[‡]https://www.nexans.nl/eservice/Netherlands-nl_NL/navigate_346195/FLAMEX_SI_EN_50382_2_Type_FXZ_3_6_6kV.html

The lifting-line model was used to compute the impact of a main propeller and distributed propellers on the wing lift and drag coefficients. The upstream effect of the wing on the propellers was ignored. Figure 3 provides a sketch of the considered propeller-wing layout, including an overview of some of the most relevant parameters.

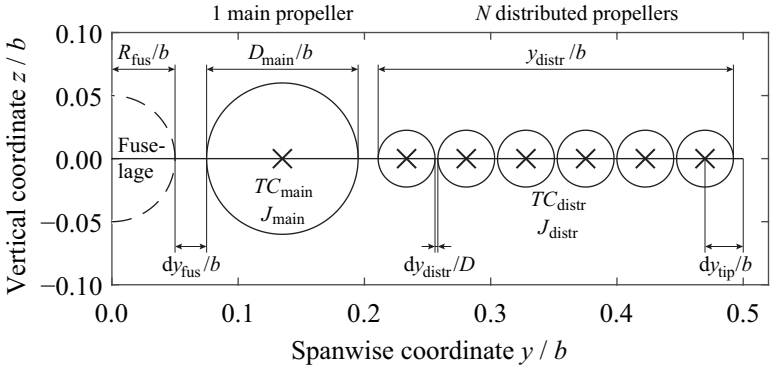

Fig. 3 Sketch of layout used in lifting-line analysis of wing-mounted tractor propellers.

Ten variables were used in the analyses. These variables are gathered in Table 3, together with the minimum and maximum values evaluated. In this table, y_{free} is the wingspan available for distributed propellers, taking into account the presence of the fuselage and main propeller, as well as clearances. The diameter of the distributed propellers follows from the selection of number of propellers, propeller-propeller spacing, and overall span of distributed propellers. Besides the selected design variables, a series of geometrical parameters were kept constant throughout the model in order to limit the number of dimensions. These parameters are shown in Table 4.

Table 3 Design variables evaluated in the lifting-line model.

Variable	Min	Max
Wing angle of attack, α [deg]	-5	30
Wing aspect ratio, AR	8	16
Diameter-to-span ratio of main propulsor, D_{main}/b	0	0.2
Thrust coefficient of main propulsor, TC_{main}	0	1
Advance ratio of main propulsor, J_{main}	0.25	2.5
Number of distributed propulsor(s) per semi-wing, N_{distr}	0	10
Thrust coefficient of distributed propulsor(s), TC_{distr}	0	1
Advance ratio of distributed propulsor(s), J_{distr}	0.25	2.5
Fraction of available span used for distributed propulsor(s), $y_{\text{distr}}/y_{\text{free}}$	0	1
Tip-offset of most outboard distributed propulsor, $dy_{\text{tip}}/y_{\text{free}}$	0	0.5

Before starting the aircraft design process, the overall lift and drag coefficients of the wing with propellers were computed for a wide range of configurations. Since the number of distributed propellers N_{distr} is a discrete variable, a Latin-hypercube sampling of 33,000 points was created for the remaining nine design variables, for each of the eleven possible N_{distr} values (see Table 3). The lifting-line model was applied for each sampling point, and the results from the different function evaluations were compared to the equivalent propeller-off solution, thus providing the lift and drag deltas (ΔC_L and ΔC_D) due to aero-propulsive interaction. To decrease runtime and ensure smooth results, a surrogate model was created based on these data points for both ΔC_L and ΔC_D for each number of distributed propellers. Each surrogate model consists of a nine-dimensional, fourth-order polynomial fit, obtained using a linear-least-squares algorithm. In the fitting process, 95% (31,350) of the points were used to construct the model, and the remaining randomly selected 5% (1,650) was used to evaluate the quality of the fit. The mean deviation of the fit over the 1,650 test points was found to be below 0.05% in all cases, although a maximum deviation in the order of 20% was found in some cases. However, such large deviations were only observed for outlying data points, and thus it was concluded that the fit was accurate for realistic combinations of input variables.

Table 4 Design parameters that were kept constant in the lifting-line model.

Parameter	Value
Wing sweep angle, Λ [deg]	0
Wing taper ratio, λ	1
Fuselage diameter with respect to wing span, R_{fus}/b	0.05
Spacing between fuselage edge and tip of main propeller, $\mathrm{d}y_{\text{fus}}/b$	0.025
Lateral spacing between propellers, $\mathrm{d}y_{\text{distr}}/D$	0.05
Axial separation between propeller plane(s) and wing leading-edge, $\mathrm{d}x/D$	0.5
Vertical offset of propellers with respect to wing chord, $\mathrm{d}z/D$	0
Propeller incidence angle, α_{props} [deg]	0

B. Boundary-layer ingestion

There are multiple ways to analyze the aerodynamic interaction that occurs between a boundary-layer-ingesting propulsor and an upstream body [42]. However, to evaluate the impact of boundary-layer ingestion (BLI) in the preliminary sizing phase, highly simplified approaches are required, which model the impact on aircraft performance in terms of parameters such as the aircraft drag coefficient, or the propulsive efficiency of the propeller or fan [27]. While several expressions have been derived which estimate the effect of BLI on "propulsive efficiency" [43, 44], these approaches are not formulated in terms of typical Class-I aircraft design parameters, and present no explicit formulation for the impact of the propeller on fuselage drag. Therefore, a simplified approach is taken which considers an actuator disk located at the end of an axisymmetric body, as depicted in Figure 4. Although the method will be described more exhaustively in future publications, a brief overview is provided in the following paragraphs.

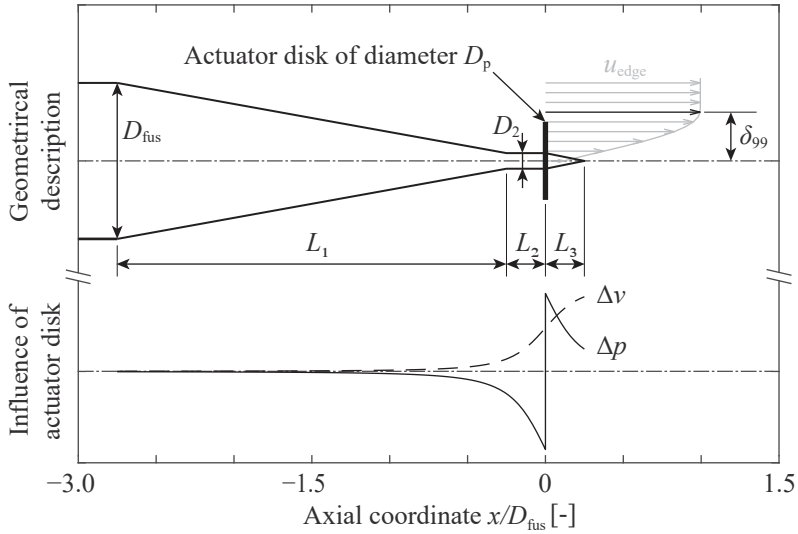

Fig. 4 Sketch of the simplified model used to estimate the impact of a fuselage-mounted boundary-layer-ingesting propeller.

In this approach, the effect of the propeller on the fuselage and vice versa are evaluated independently, and no iterative dependencies are considered. Since the problem is assumed to be axisymmetric, the influence of the wing, empennage, or tail-cone upsweep are not considered. Moreover, the flow on the fuselage is assumed to be attached. The fuselage geometry is simplified and discretized into three sections: the "main" tail-cone of the fuselage, of length L_1, a cylindrical segment of length L_2 and diameter D_2—at the end of which the propeller of diameter D_p is located—and a final conical section of length L_3, which represents the spinner behind the propeller. The dimensions, shown in the top half of Figure 4, must be chosen by the designer and expressed as a fraction of the fuselage diameter D_{fus}, since in the conceptual design process the actual dimensions of the aircraft are unknown.

The effect of BLI on propeller performance is estimated by introducing the concept of an isolated (i.e., uninstalled) *equivalent freestream actuator*, operating at a uniform inflow velocity V_{eq} and freestream static pressure p_∞. The equivalent velocity V_{eq} is computed taking into account two contributions: the average inflow velocity at the location of the (installed) actuator disk, and the average static pressure at that same location. The first is computed by assuming a boundary-layer velocity profile $V(r)/V_{\text{edge}} = f(r/\delta_{99})$ and taking the mean over the propeller disk by integrating this profile over cylindrical coordinates. The second, determined by the pressure coefficient at the end of the fuselage, is translated into an effective velocity increase at the actuator disk by assuming that the increased static pressure at the upstream end of the actuator's stream tube is isentropically expanded to ambient pressure. The edge velocity of the boundary layer V_{edge}, the boundary layer thickness δ_{99}, and the pressure coefficient at the fuselage trailing edge (which is directly related to the edge velocity), are estimated using the data presented in Refs. [45, 46] The boundary layer profile is based on experimental data obtained by Della Corte in the CENTRELINE[§] research project (see e.g. Ref. [47]), using the experimental setup used by Lv et al. [25] The propulsive efficiency of the equivalent freestream actuator is then compared to an actuator disk producing the same thrust in ambient conditions (V_∞, p_∞) to compute the effective change in propulsive efficiency due to BLI, $\Delta\eta_{\text{p}}$.

Finally, the effect of the propeller on fuselage drag is estimated taking into account two contributions. The first is the change in pressure drag on the fuselage tail-cone due to the propeller-induced static pressure field. The second is the change in friction drag due to the increased shear in the boundary layer near the fuselage surface, as a result of the propeller-induced velocity increase. It is assumed that the propeller—which is uniformly loaded—does not affect the shape or thickness of the boundary layer, but simply scales the velocities near the surface as if the edge velocity were scaled with a factor $(V_{\text{edge}} + \Delta V)/V_{\text{edge}}$. Therefore, the change in pressure drag due to a reduced boundary-layer thickness, or the change in friction drag due to a change in the boundary-layer profile, are not considered. The changes in velocity (ΔV) and static pressure (Δp) upstream of the propeller are notionally indicated in the bottom half of Figure 4, and are estimated using actuator-disk theory. These variations are then integrated over the tail-cone surface to obtain the total change in drag. This drag increase is then included as a change in zero-lift drag coefficient, ΔC_{D0}, in the aircraft design process.

IV. Reference aircraft and case study definitions

As reference configurations, conventional tube and wing aircraft with wing-mounted propellers were designed using the Initiator. Validation studies of the design software have been performed for both an ATR-72 and Fokker 50, as presented by Schouten et al. [48]. These designs are repeated for the current design exercise, given the slightly different sizing process.

A. Comparison to reference data

The resulting performance, dimensions and weights are compared to values found in open literature, with the aim to demonstrate that the aircraft design process results in conceptual aircraft designs that are relatively close to existing aircraft. The top-level aircraft requirements (TLARs) for these designs have been derived from publicly available data[¶‖**] and are summarized in Table 5.

Figure 5 presents the geometry of converged aircraft produced by the Initiator for the TLARS in Table 5. A more quantitative comparison on some of the overall vehicle characteristics is presented in Table 6. It can also be seen that the maximum take-off mass (MTOM) of both aircraft is within 5% of the reference values.

The difference in OEM for the ATR is related to the large over-estimation of maximum power in one-engine-inoperative (OEI) conditions; the OEM difference in the case of the F50 is related to a combination of slightly overestimated engine size as well as underestimated wing area. The simplified engine model also leads to an underestimation of the mission fuel. The differences are within the range of variations typically seen for conceptual aircraft design, but should be noted when comparing results of various configurations between each other.

[§]CENTRELINE - ConcEpt validatioN sTudy foR fusElage wakefilLIng propulsioN integration, EU Horizon 2020 project Grant Agreement No. 723242

[¶]`https://janes.ihs.com/JAWADevelopmentProduction`

[‖]`www.flyfokker.com`

[**]`www.atraircraft.com`

Table 5 TLARs for reference aircraft. Data from Jane's and Fokker/ATR documentation.

Spec.	Unit	ATR-72 (alternative mission)	F-50 (alternative mission)
Harmonic range	km	926 (1530)	1089 (1675)
Structural payload	kg	7500 (6650)	5500 (4850)
Passengers	-	70	50
Cruise altitude	m	7000	7620
Cruise Mach	-	0.41	0.46
Take-off distance	m	1333	1095
Approach speed	m/s	58.1	51.4

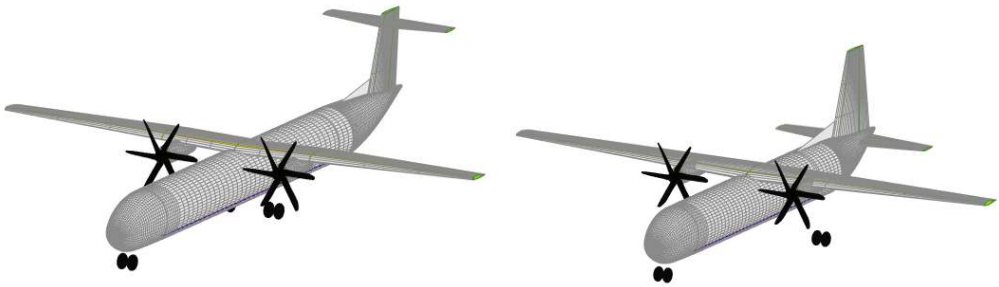

(a) ATR 72-600(I) (b) Fokker 50(I)

Fig. 5 Isometric view of aircraft designs produced by the Initiator.

Table 6 Comparison of Initiator results to published data of the ATR 72-600 and Fokker 50. Data from Jane's, ATR and Fokker.

		ATR 72-600			Fokker 50		
	unit	Reference	Initiator	Difference	Reference	Initiator	Difference
MTOM	t	22.8	22.9	0.5%	19.9	18.9	-5.0%
OEM	t	13.3	14.1	6.0%	12.5	12.4	-1.0%
Total P_{max}	kW	4100	4597	12.1%	3720	3813	2.5%
W_{max}/P_{max}	N/kW	54.6	48.6	-11%	51.2	48.7	-4.9%
W/S_w	N/m^2	3670	3690	4.3%	2795	2995	7.2%
S_w	m^2	61	60.5	-1.0%	70	62	-11.4%
b_w	m	27	27	0.0%	29	27.3	-5.8%
l_f	m	27.2	28.8	5.9%	25	23	-8.0%
d_f	m	2.9	2.8	-3.4%	2.7	2.8	3.7%
d_p	m	3.9	4.1	5.1%	3.7	3.9	5.4%

B. Top-Level Aircraft Requirements for DHEP study

A set of top-level aircraft requirements (TLARs) has been defined for LPA WP1.6.1.4. These TLARs are roughly based on an Airbus A320, with some modifications in terms of range, cruise speed and altitude, based on the findings of Refs.[13, 28] These requirements are listed in Table 7.

To cover a broader area in the design space, the design studies presented in this article cover harmonic ranges of both 1100nmi and 2000nmi and a variety of cruise Mach numbers, ranging from 0.6 down to 0.5. All aircraft are assessed for different (10 to 30%) shaft power ratios (φ) and "technology scenarios" (low, medium, high) for powertrain components as presented in Table 8.

Table 7 Top-level aircraft requirements for hybrid electric aircraft as defined in LPA WP1.6.1.4.

Parameter	Unit	Required Value	Condition
Harmonic range	nmi	1100	
Maximum payload	kg	20000	
DOC mission	nmi	800	
DOC payload	kg	15000	
Diversion range	nmi	250	$M = 0.45; h =$ FL150
(Initial) Cruise Mach number	-	0.6	
Initial Cruise Altitude (ICA)	ft	25000	after T/O @ MTOM, ISA+10°
Time-to-climb from 1500 ft. to ICA (TT)	min	35	after T/O @ MTOM, ISA+10°
Take-off Field Length (TOFL)	m	2200	@ SL, ISA+15°
Approach speed (landing)	KCAS	138	
Wing span limit	m	52	
One-engine-out (OEI) net ceiling	ft	15000	
Loiter time	min	30	
MLM (% MTOM)	-	100	
BC/YC	-	12/138	
Service life/cycles	-	100,000	

Table 8 Hypothetical technology scenarios for powertrain components, with constant transmission efficiencies.

Scenario	**Electrical machines**	**Gas turbines**
	ESP [kW/kg]	SP [kW/kg]
Low	3.7	3.5
Med	5.4	7.0
High	9.1	10.5

C. Reference aircraft

Based on the TLARs presented in Table 7, three reference configurations are generated using the Initiator design process. These aircraft (for the low technology scenario) are shown in Figure 6 and represent the three propulsion system layouts without distributed electric propulsion. The WMP, HTMP and FMDP configurations are in line with those presented by Vos and Hoogreef [26]. They are used here to identify what benefits DHEP can bring to more unconventional aircraft concepts and to verify whether a benefit/penalty of any secondary propulsion system is actually related to the layout of the primary propulsion system. All these reference aircraft will be shown in the analysis of results, where they will be designed according to the same technology levels as those with DHEP.

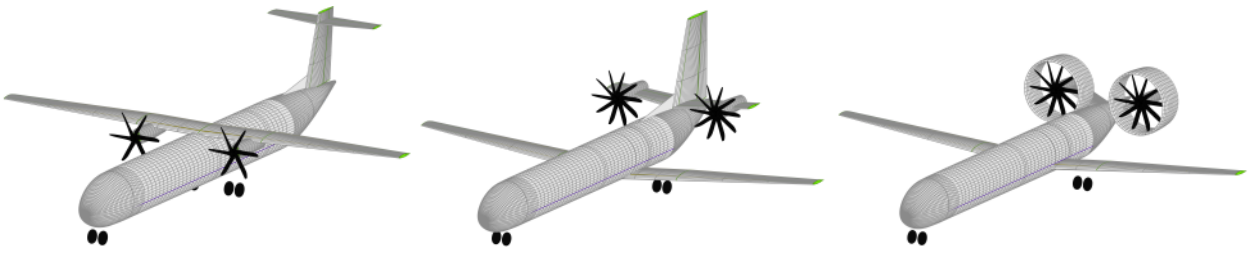

(a) WMP reference aircraft (b) HTMP reference aircraft (c) FMDP reference aircraft

Fig. 6 Isometric views of three reference aircraft designs produced by the Initiator.

An overview of some quantitative vehicle characteristics of the aircraft shown in Figure 6 is presented in Table 9, where it is immediately clear that the WMP outperforms the other two aircraft. These results are in line with those found in [26], although the TLARs are slightly different and a stability/controllability assessment is not included in the current design process. Still, the aft-located CG of HTMP and FMDP concepts has a significant influence on the overall aerodynamic performance of the aircraft (due to trimming) and overall weight. The higher wing loading of the WMP can be attributed to the use of the lifting line model for the (beneficial) aero-propulsive interaction of the two main, wing-mounted, propellers.

Table 9 Initiator results for the WMP, HTMP and FMDP reference aircraft without distributed electric propulsion, with conventional powertrain and low technology scenario gas turbine performance, including aero-propulsive effects of wing-mounted main engines.

	Unit	WMP	HTMP	FDMP
MTOM	t	58.9	65.5	69.2
OEM	t	33.5	39.1	42.9
Total P_{max}	MW	13.9	16.5	17.1
W_{max}/P_{max}	N/kW	41.5	38.9	39.8
W/S_w	N/m^2	5857	5510	5510
S_w	m^2	98.7	116.6	123.1
b_w	m	34.4	37.4	38.4
l_f	m	37.7	37.7	37.7
d_f	m	3.9	3.9	3.9
d_p	m	4.3	4.8	5.0

D. Aircraft configurations with distributed propulsion

All envisioned aircraft configurations shown in Figure 6 are combined with a secondary set of propulsors, in addition to a primary propulsive device with the aim of leveraging beneficial aero-propulsive interaction effects. All these configurations use a partial turbo-electric architecture (i.e. without batteries), have a constant span fraction for DHEP (per type of secondary propulsors), constant shaft power ratio over all mission phases and a constrained helicoidal tip Mach number for the propellers. Figures 7, 8 and 9 illustrate all the different layouts that have been evaluated: tip-mounted propellers, eight and ten LE distributed propellers (covering the same span fraction) and a BLI fan for the WMP case (as it is not considered effective for the other primary propulsion chain layouts due to the location of the engines).

V. Analysis of results

Over 600 Initiator design convergence studies were performed, for different cruise Mach numbers and harmonic ranges. For the baseline requirements, some additional studies were made for larger tip-mounted propellers, even better technologies for the electrical machines and even lower shaft power ratio (5%) to confirm some of the convergence behavior. It should be noted that not all combinations yielded feasible results due to limitations of the range of the surrogate models used for the aero-propulsive interactions (lower Mach numbers were tested, but did not provide feasible results) and due to the fact that the configurations are not optimized. Therefore, the results should be treated carefully and should be used to set a directive for future studies on aircraft system level (more optimal aircraft setup/TLAR for DHEP), necessary high-fidelity detail studies (to enrich the surrogate models) and necessary inclusions of additional (inter-)disciplinary effects. It is important to remember that the configurations as such are a direct consequence of the selected DHEP technology (BLI, LE distributed or tip-mounted propulsion) and the resulting concepts are feasible, but not optimal, designs. Thus, conclusions can be made on interesting application areas of technology, rather than on resulting aircraft concepts.

At aircraft level, two output parameters are of primary interest: maximum take-off mass (MTOM) and payload-range energy efficiency (PREE) [13, 49]. The latter is used as figure-of-merit, representing the overall energy efficiency of the aircraft in transporting payload over a certain range. It can be written in non-dimensional form and is inversely

proportional to the amount of energy consumed for a given mission segment (in this case only the harmonic mission excluding reserves):

$$\text{PREE} = \frac{W_{\text{PL}} R}{E_{\text{miss}}}. \tag{8}$$

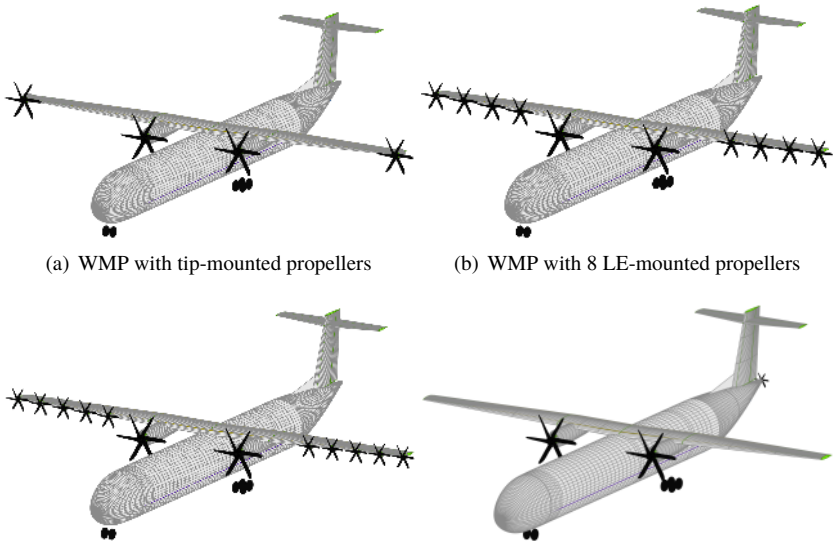

(a) WMP with tip-mounted propellers (b) WMP with 8 LE-mounted propellers

(c) WMP with 10 LE-mounted propellers (d) WMP with wake-ingesting (BLI) fan

Fig. 7 Isometric views of WMP aircraft with different forms of partial turbo-electric distributed propulsion as produced by the Initiator. Note that only landing gear position (not length) is shown.

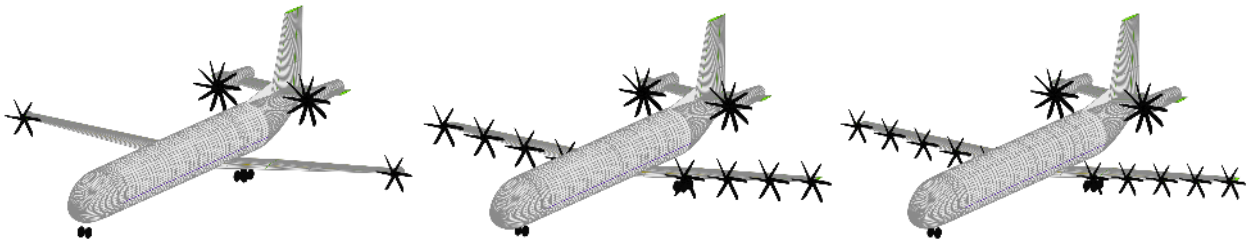

(a) HTMP with tip-mounted propellers (b) HTMP with 8 LE-mounted propellers (c) HTMP with 10 LE-mounted propellers

Fig. 8 Isometric views of HTMP aircraft with different forms of partial turbo-electric distributed propulsion as produced by the Initiator. Note that only landing gear position (not length) is shown.

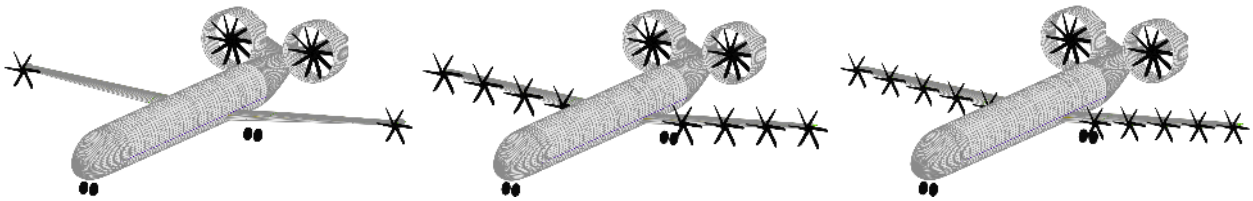

(a) FMDP with tip-mounted propellers (b) FMDP with 8 LE-mounted propellers (c) FMDP with 10 LE-mounted propellers

Fig. 9 Isometric views of FMDP aircraft with different forms of partial turbo-electric distributed propulsion as produced by the Initiator. Note that only landing gear position (not length) is shown.

A. Effect of shaft power ratio and technology scenario

The baseline mission according to the TLARs of Table 7 specifies a harmonic range of 1100nmi and a cruise Mach number of 0.6. For this mission, 99 different aircraft were synthesized for different technology scenarios and different shaft power ratios (φ). The results are presented in Figure 10 according to their PREE and MTOM, where different φ-values are represented by a different color shade. The reference aircraft have always been evaluated for the same technology level as the DHEP configurations.

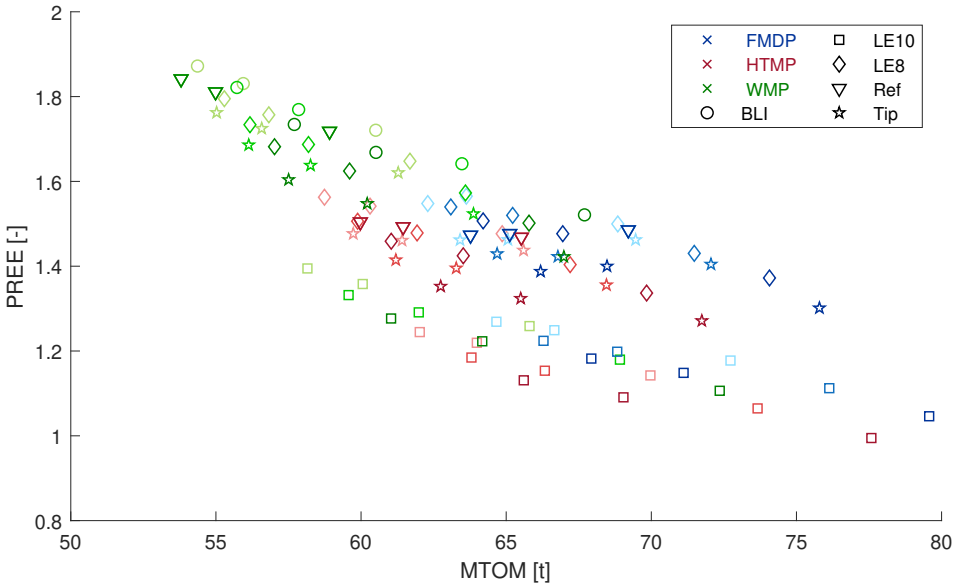

Fig. 10 Overview of PREE vs MTOM for 10-30% φ and technology scenarios for R = 1100nmi and M = 0.6. Lighter color shades indicate lower φ.

Figure 10 shows a large spread in both PREE and MTOM, with in general the same trends for MTOM as was calculated for the reference aircraft. It is immediately obvious that the lower shaft power ratios show better results, with both higher PREE and lower MTOM. The BLI aircraft seem to be able to achieve a slightly higher PREE, at the cost of a slight increase in MTOM (due to the additional powertrain components). The other DHEP technologies seem to approach a PREE close to that of their respective reference, yet also at higher MTOMs. It is important to note that there is significant room for improving the setup of the DHEP configurations that were tested as well as their operating altitude. As shown in [13], this can have a significant impact on the results.

The large difference between eight and ten leading-edge distributed propellers is unexpected. Although it is expected that more smaller propellers perform worse than fewer larger ones for the same wingspan covered, this large difference was not expected. As will be shown later, aircraft with ten distributed propellers have significantly higher powertrain masses. In addition, their operating point is far from optimal, leading to high advance ratios and low aero-propulsive benefits..

The BLI configuration seems to perform particularly well, though only at very low shaft-power ratios. This benefit confirms the potential of BLI, and thus additional higher-fidelity studies of this configuration are required.

To better illustrate the separate effects of technology scenario and φ, Figure 11 and Figure 12 present the resulting PREE and MTOM for a sweep of technology scenarios and a sweep of shaft power ratios, respectively. It can be seen from these figures that the influence of technology scenario is mostly on MTOM (in fact, powertrain mass) of the aircraft, which to a lesser extent influences PREE. The shaft power ratio has a significant effect on both PREE and MTOM, showing that beyond 20% shaft power ratio, PREE decreases and MTOM increases much more than between 10% and 20%. The higher shaft power ratio has of course a large effect on powertrain mass, which incurs a cyclic effect on MTOM. However, as will be shown in sub-Section V.C, there is also a decrease in aero-propulsive efficiency.

The low performance of the tip-mounted propulsion system was not expected and further investigations showed that at the high cruise Mach number of 0.6, the advance ratio of the tip-mounted system was constrained by the tip Mach number. For the selected reference blade loading distribution, this resulted in high advance ratios and low thrust coefficients, which led to a small (friction) drag penalty.

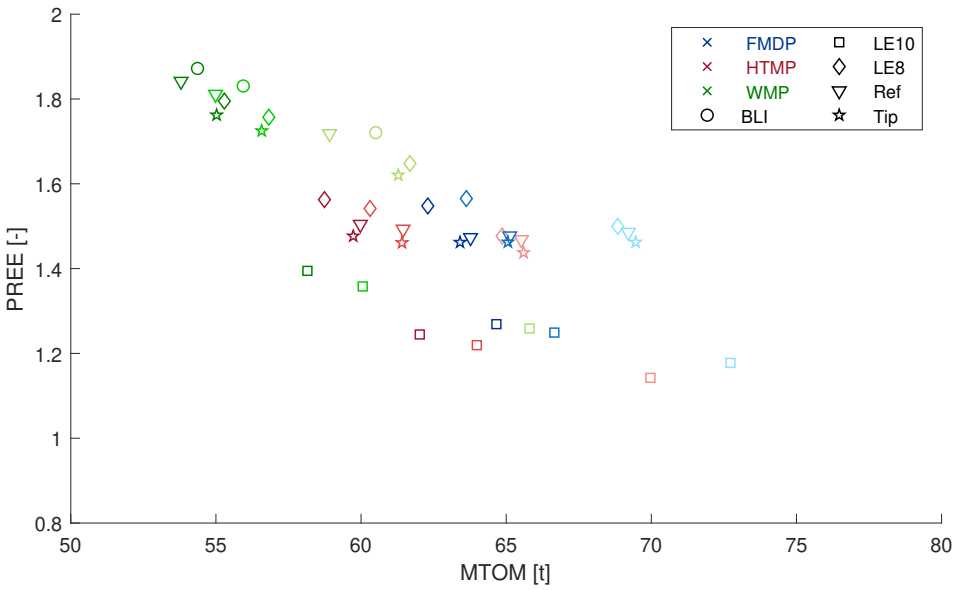

Fig. 11 Overview of PREE vs MTOM for 10% φ and variable technology scenarios for R = 1100nmi and M = 0.6. Lighter color shades indicate lower technology scenarios.

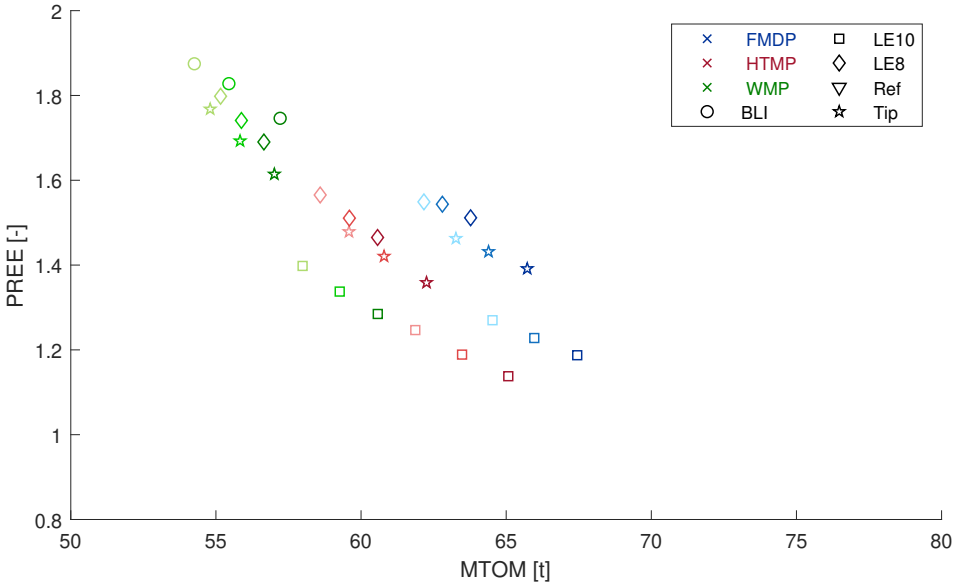

Fig. 12 Overview of PREE vs MTOM for 10-30% φ and high technology scenario for R = 1100nmi and M = 0.6. Lighter color shades indicate lower φ.

Similar to the shaft power ratio, the difference between higher and lower technology scenarios is larger between low and medium than medium and high, even though the step in improved component specific power is smaller! Figures 13 and 14 show the results of additional investigations into the effects of even larger specific powers (technology scenario) and an even lower shaft power ratio.

From Figure 13 it is clear that, obviously, the improved technology has more effect on larger shaft power ratios. However, similar to the trends in Figure 11, an extreme improvement on the specific power of the powertrain components does not yield an as-extreme improvement on aircraft level. This can be explained by the fact that the fraction of the powertrain mass of the OEM becomes smaller with improving powertrain technology. Therefore, a further improvement has even less of an impact with respect to the other parts that make up the OEM (and MTOM). As such, the medium

technology scenario of Table 8 appears to yield results that should be obtainable in the near future, though ideally combined with a low φ.

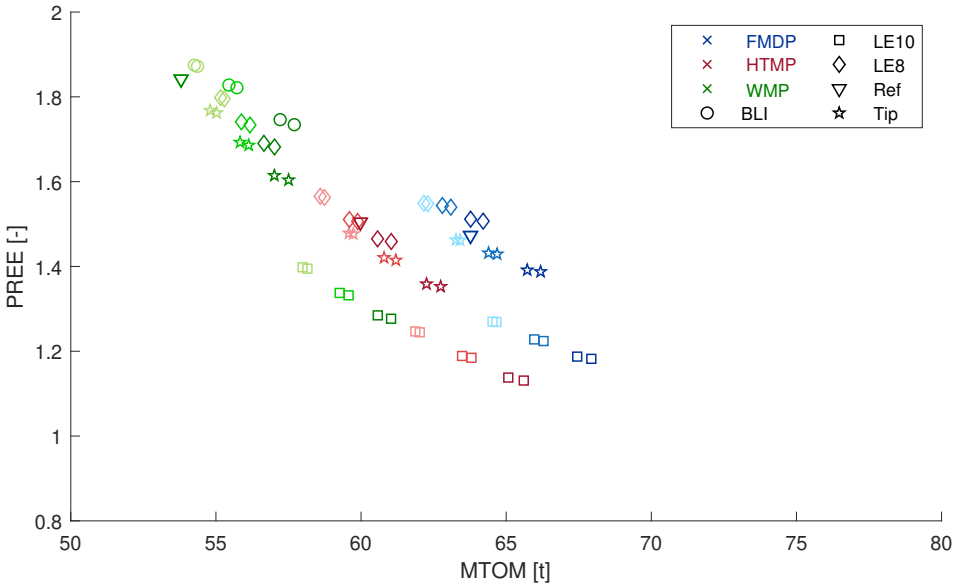

Fig. 13 Overview of PREE vs MTOM for 10-30% φ and extra high (12.4 kW/kg) electromotor technology for R = 1100nmi and M = 0.6. Lighter color shades indicate lower φ.

An even lower shaft power ratio, as shown in Figure 14, shows a (very) small improvement for the two aircraft layouts with aft-mounted main propulsors. However, importantly, for the more conventional layout with wing-mounted main propulsors, little to no benefit is achieved. Likely, this is caused by the fact that the secondary propulsors are so small that they do impose a mass penalty yet yield no aero-propulsive benefit.

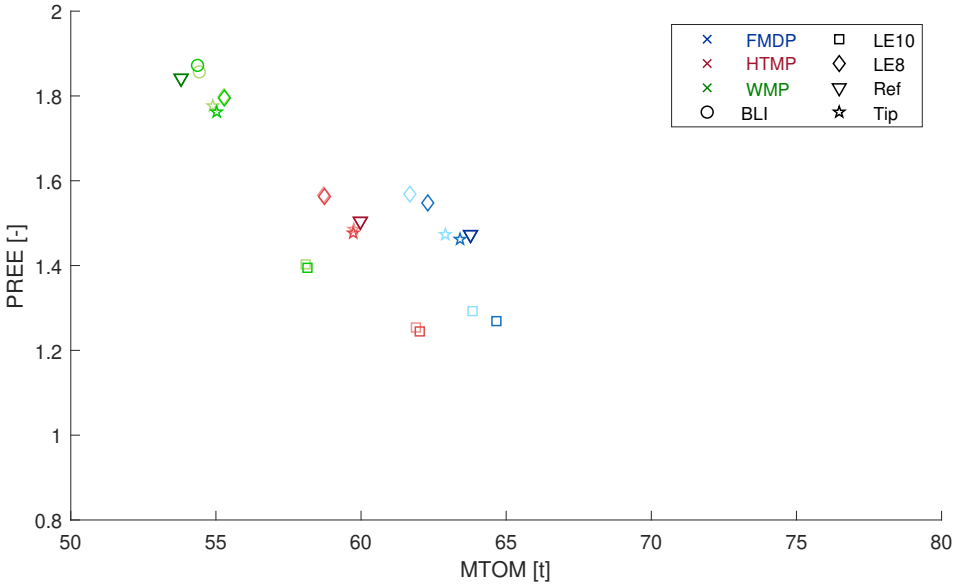

Fig. 14 Overview of PREE vs MTOM for 5 and 10% φ and high technology scenario for R = 1100nmi and M = 0.6. Lighter color shades indicate lower φ.

B. Effect of altitude and range

Figure 15 presents the results for the same aircraft configurations designed for varying harmonic range (1100 and 2000 nmi) and varying cruise Mach number (0.5 and 0.6). The results shown here are limited to the high technology scenario and $\varphi = 10\%$. It must be noted that for the long-range case at low speed, the FMDP aircraft showed convergence issues. The results show that in general a longer range leads to a higher PREE, especially for those aircraft with a secondary powertrain as the beneficial aero-propulsive effects can act over a longer duration, to overcome the increased mass due to the secondary propulsion system. Similarly, at lower speeds all aircraft are more efficient thanks to the aero-propulsive interactions (tip speed limited) being more favorable at lower speeds. Particularly the case with ten LE distributed propellers seems to benefit from the change from Mach 0.6 to Mach 0.5. At the high range case for Mach 0.5, it can be seen that the distributed propulsion systems show the largest improvement.

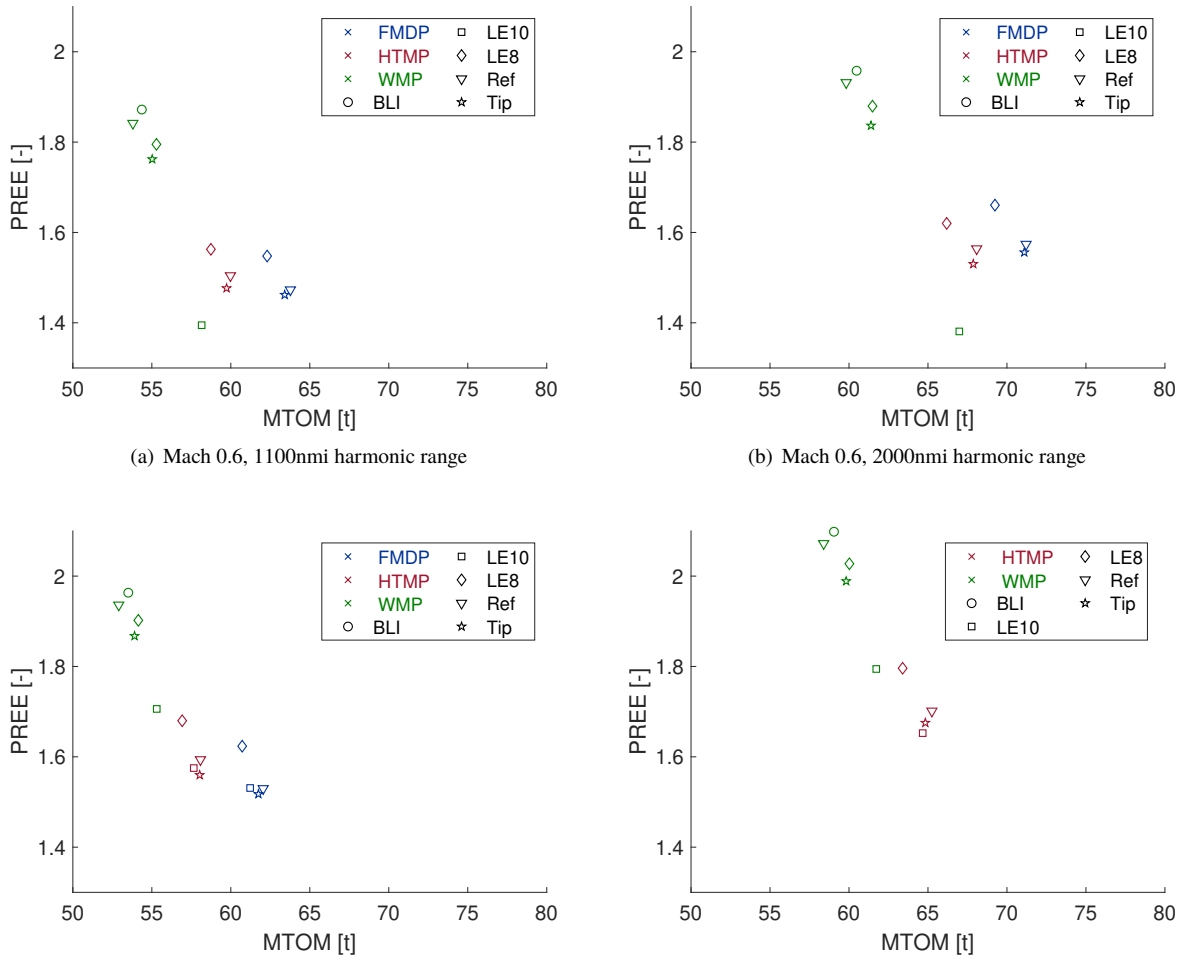

(a) Mach 0.6, 1100nmi harmonic range

(b) Mach 0.6, 2000nmi harmonic range

(c) Mach 0.5, 1100nmi harmonic range

(d) Mach 0.5, 2000nmi harmonic range

Fig. 15 Illustration of effects of harmonic range and cruise Mach number on PREE and MTOM for high technology scenario and 10% φ.

C. Aero-propulsive efficiency

The PREE is largely influenced by the aero-propulsive efficiency of the aircraft, which can be expressed as $(\eta_p \cdot L/D)$, where η_p is calculated as the weighted average between the two propulsion chains for their respective power share. Figure 16 illustrates the resulting aero-propulsive efficiency for the baseline mission requirements and varying shaft power ratio. The results show that, except for the tip-mounted cases and concepts with ten LE distributed propellers, the DHEP configurations perform well with respect to the reference aircraft, confirming that they perform better on longer ranges. The slightly worse performance of the tip-mounted propellers is again attributed to the high advance ratio, for

which the loading distribution assumed here was not optimized for. Consequently, the propeller swirl was not optimal for maximum induced drag reduction, and in fact the increased axial velocity in the slipstream caused a drag increment due to friction. Figures 17 and 18 show that the DHEP configurations do yield a marginally larger overall propulsive efficiency and aerodynamic efficiency, yet not enough to generate a significantly larger aero-propulsive efficiency.

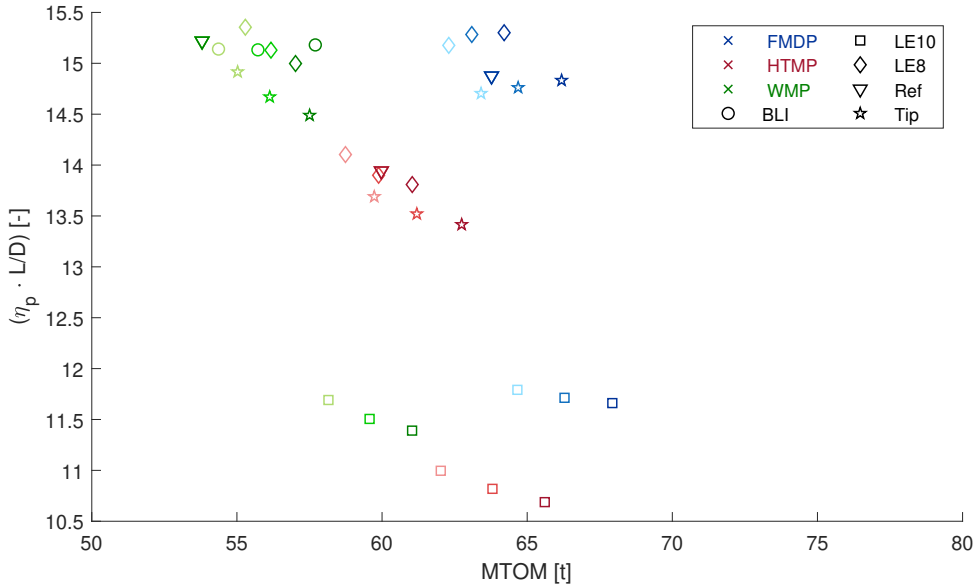

Fig. 16 Overview of ($\eta_p \cdot$ L/D) vs MTOM for 10-30% φ and high technology scenario for R = 1100nmi and M = 0.6. Lighter color shades indicate lower φ.

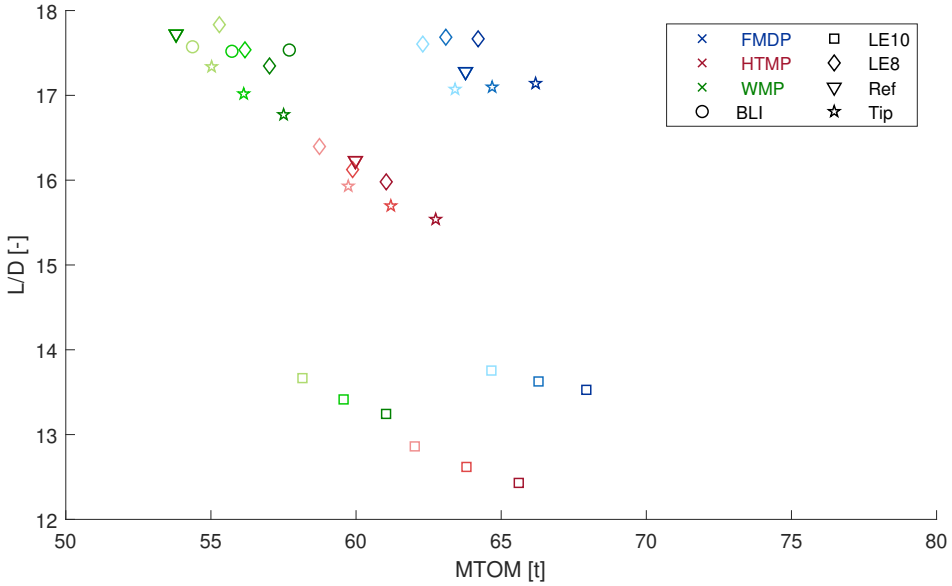

Fig. 17 Overview of L/D vs MTOM for 10-30% φ and high technology scenario for R = 1100nmi and M = 0.6. Lighter color shades indicate lower φ.

An investigation of the aero-propulsive efficiency for aircraft designed for longer ranges and lower cruise Mach numbers shows that a longer harmonic range has very little effect on ($\eta_p \cdot$ L/D), as expected. The value of ($\eta_p \cdot$ L/D) has more of an effect on the energy consumption of the aircraft over the longer range, as shown in Figure 19.

The difference of lowering the cruise speed is significant though, as shown in Figure 20, highlighting improved

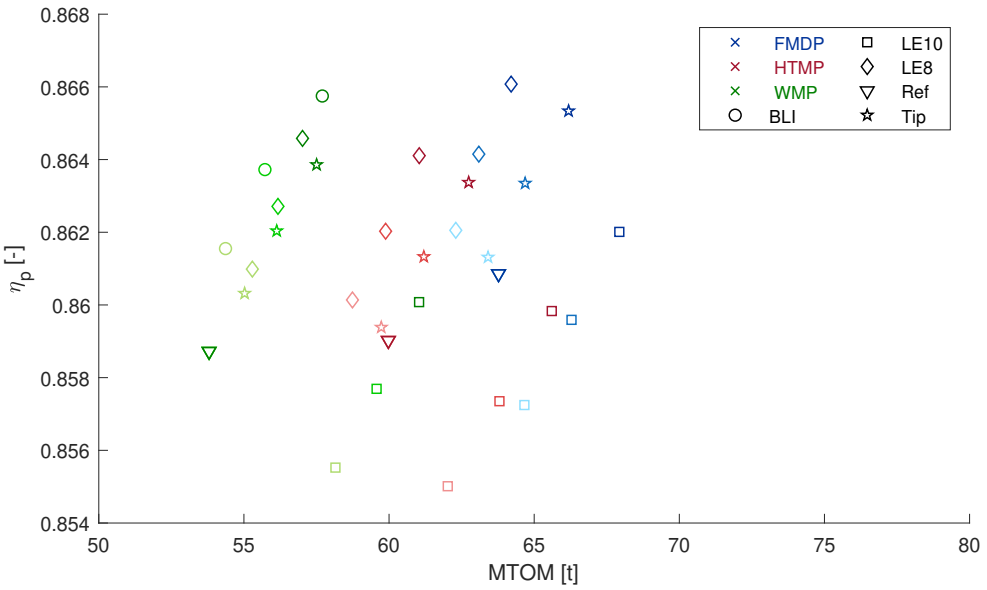

Fig. 18 Overview of η_p vs MTOM for 10-30% φ and high technology scenario for R = 1100nmi and M = 0.6. Lighter color shades indicate lower φ.

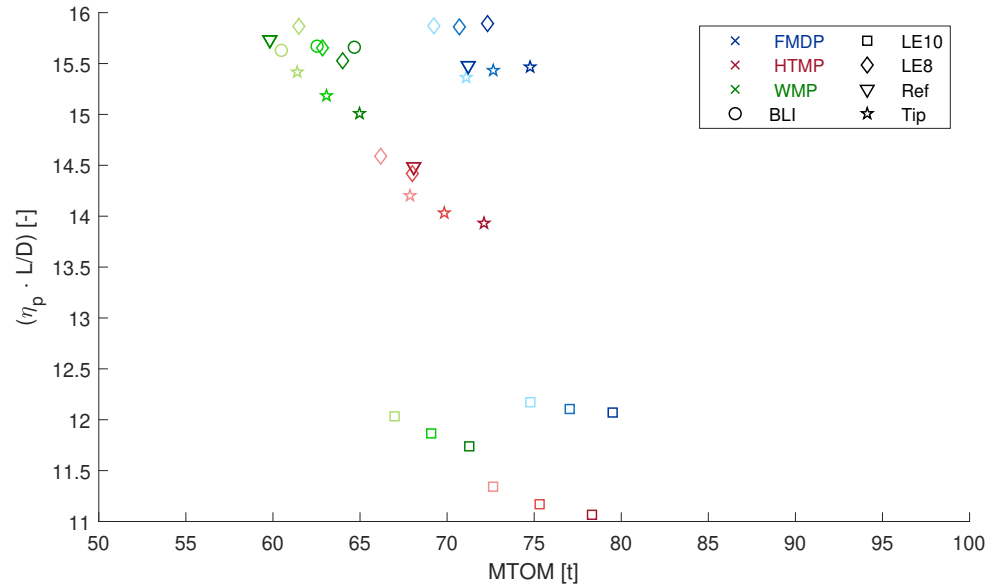

Fig. 19 Overview of $(\eta_p \cdot L/D)$ vs MTOM for 10-30% φ and high technology scenario for R = 2000nmi and M = 0.6. Lighter color shades indicate lower φ.

performance for the DHEP configurations. Again, the effect on MTOM of the different shaft power ratios is largely related to the additional powertrain mass.

D. Effect on weight breakdown

In terms of structure, the installation of multiple propellers on the wing can have both a beneficial effect (wing bending relief) and a negative effect (additional masses amount to additional required structure in unloaded conditions), it is interesting to investigate the effects of DHEP on the wing mass for varying shaft power ratios. Note that the wing mass does not include the distributed propulsion system or cables themselves. In Figure 21, it can be seen that the

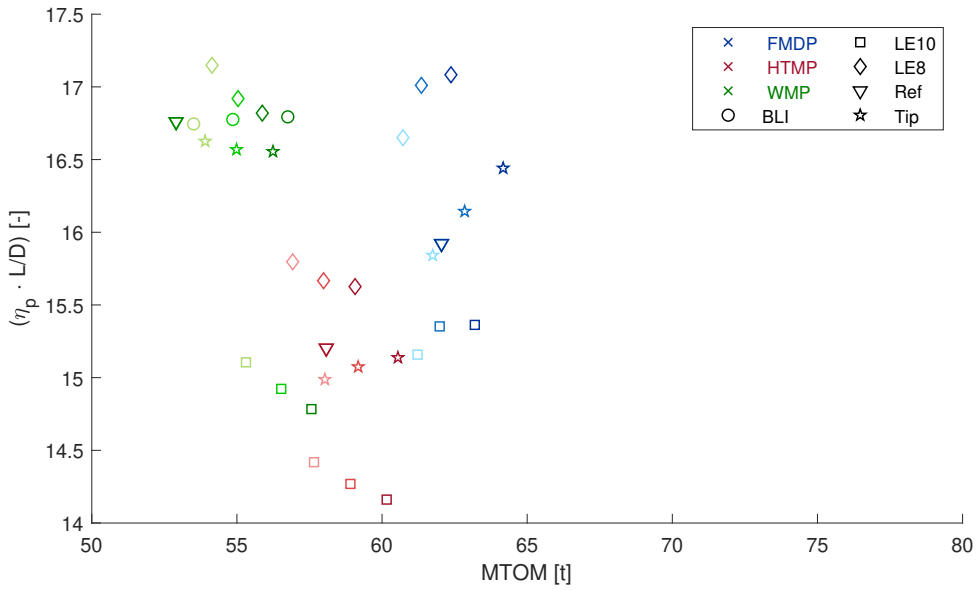

Fig. 20 Overview of $(\eta_p \cdot L/D)$ vs MTOM for 10-30% φ and high technology scenario for R = 1100nmi and M = 0.5. Lighter color shades indicate lower φ.

influence of higher shaft power ratios is present on the wing mass, but not dominating. The large difference between FMDP and HTMP is due to a combination of wing position an overall MTOM.

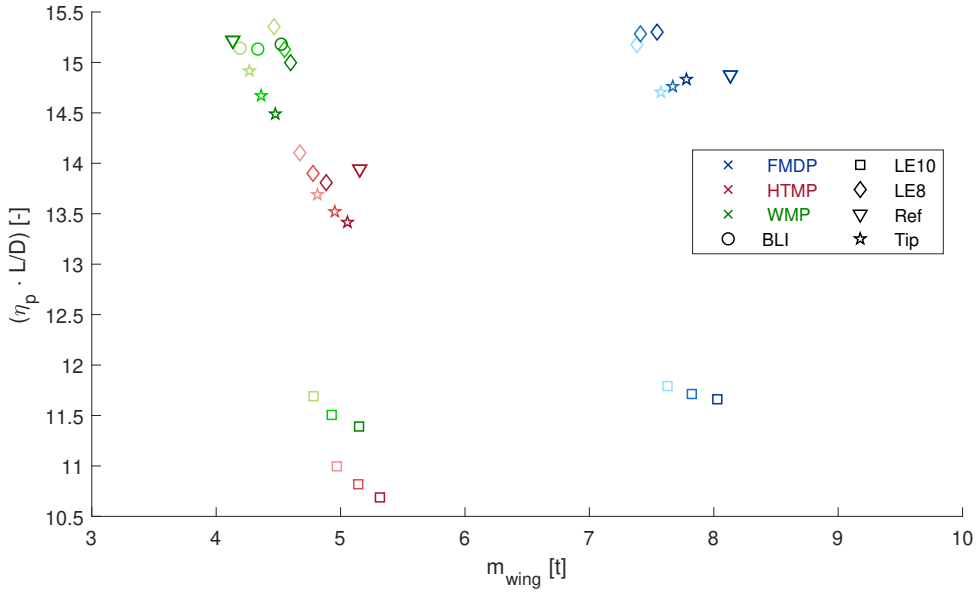

Fig. 21 Overview of $(\eta_p \cdot L/D)$ vs wing mass for 10-30% φ and high technology scenario for R = 1100nmi and M = 0.6. Lighter color shades indicate lower φ.

In fact, when studying Figure 22, it can be seen that the powertrain mass is significantly more influenced. A further investigation of the wing mass estimation performed by the FEM wing weight tool inside the Initiator design loop shows that multiple distributed masses lead to lower primary structure masses. However, the mass penalty associated with additional pylons and mounting points for multiple propellers leads to a higher overall wing mass. This penalty is empirical and should be further investigated.

From Figures 21 and 22 it can also be seen that for the BLI configuration, the wing mass increases much more

with increasing shaft power ratio due to the increased generator mass and the lack of additional bending relief due to distributed propellers. This increase in wing mass is also largely related to the secondary structure that is empirically sized. To illustrate the aero-propulsive effects, Table 10 provides insight into the contributions of the secondary

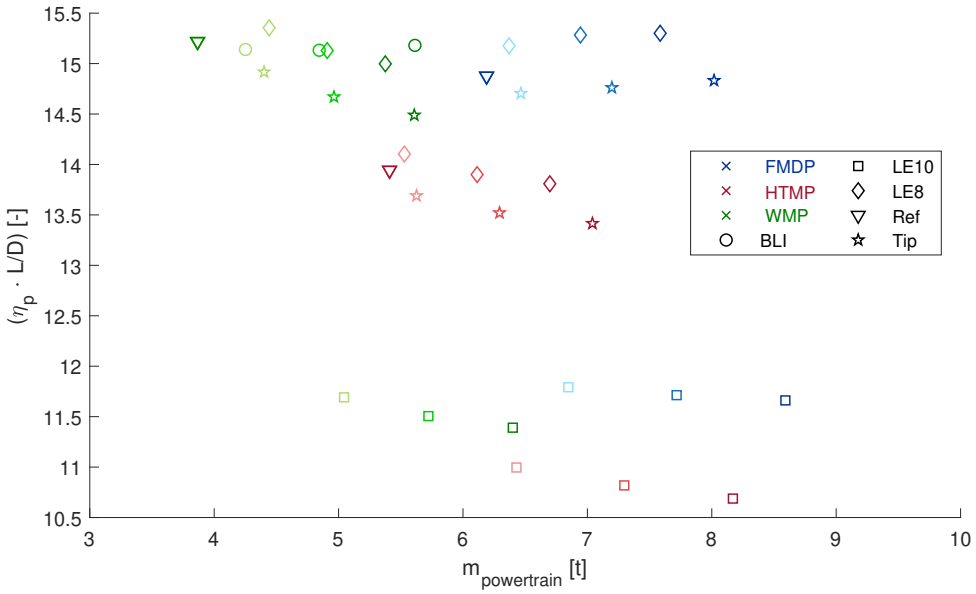

Fig. 22 Overview of $(\eta_p \cdot L/D)$ vs powertrain mass for 10-30% φ and high technology scenario for R = 1100nmi and M = 0.6. Lighter color shades indicate lower φ.

propulsion systems in terms of aerodynamic coefficients and overall propulsive efficiency, per mission phase. This table clearly shows that at lower speeds, the aero-propulsive interactions between the secondary propulsion system and the wing provide significant aerodynamic benefits. In fact, both in landing and take-off, significant increases in lifting capability and reductions in drag are visible. However, due to the rather large take-off distance and rather mild approach speed constraints (typical for turbofan aircraft), these conditions do not become sizing constraints for the aircraft design point. Therefore, the overall improvements are limited/not visible. The designs are actually cruise limited, or limited by the performance in a balked-landing with one of the main engines inoperative.

However, in the cruise phase, the design speed of Mach 0.6 is too high to result in any appreciable benefit of distributed propeller-driven secondary propulsion. The BLI propulsion system is the only resulting in any benefit in the cruise phase in terms of propulsive efficiency. The configuration with this secondary system also shows improved lift and drag (in all phases), however, these are not caused by the BLI system, but they are a result of the aero-propulsive interaction of the primary propulsive device and the main wing. The BLI system itself results in a drag penalty.

The results from Table 10 indicate that future investigations should focus on even lower speed applications. Especially for ten LE distributed propellers, the drag penalty in cruise outweighs any lift improvement. This indicates also that the designs are severely limited by the high cruise speed (for propellers).

VI. Conclusions and directions for future research

From the various studies where shaft power ratios were varied for different technology scenarios and aircraft layouts, it can be concluded that lower shaft power ratios show better results, with both higher PREE and lower MTOM. BLI aircraft seem to be able to achieve a slightly higher PREE, at the cost of a slight increase in MTOM (due to the shaft power off-take and additional powertrain components). The other DHEP technologies seem to approach a PREE close to that of their respective reference, yet also at higher MTOMs. The shaft power ratio has a significant effect on both PREE and MTOM, and it was shown that beyond 20% shaft power ratio, PREE decreases and MTOM increases much more than between 10% and 20% indicating a possible local optimum between the latter two values as even lower values did not yield any significant improvements. Tip-mounted propulsion systems performed worse than expected due to the advance ratio of the tip-mounted system being constrained by the helicoidal tip Mach number for which the loading distribution assumed here was not optimized for. Consequently, the propeller swirl was not optimal for

Table 10 Initiator results for the WMP with high technology scenario and 10% φ, showing the aero-propulsive impact for cruise, take-off and landing phases for aircraft designed for 1100nmi and M0.6. Delta values for lift and drag coefficient with respect to isolated wing case, η_p computed as weighted average. 1 drag count = 0.0001, 1 lift count = 0.01

Phase	Parameter	Unit	WMP + BLI	WMP + LE10	WMP + LE8	WMP + Tip
Cruise	$\Delta_{C_{D_i}}$	counts	0	86	-8	1
	Δ_{C_L}	counts	0.30	0.85	1.1	0.29
	η_p	%	90.3%	85.8%	86.3%	86.1%
	L/D_{iso}	-	17.5	17.3	17.0	17.3
	L/D	-	17.6	13.7	17.8	17.3
Landing	$\Delta_{C_{D_i}}$	counts	-88	-168	-66	-140
	Δ_{C_L}	counts	16	18	18	19
	η_p	%	74.0%	76.2%	76.0%	75.1%
	L/D_{iso}	-	9.6	9.5	9.5	9.6
	L/D	-	10.5	10.8	10.4	10.7
Take-off	$\Delta_{C_{D_i}}$	counts	-63	-90	-57	-74
	Δ_{C_L}	counts	11	14	13	14
	η_p	%	75.0%	75.0%	75.0%	73.9%
	L/D_{iso}	-	13.1	13.0	13.0	13.0
	L/D	-	14.6	15.1	14.6	14.9

maximum induced drag reduction, and in fact the increased axial velocity in the slipstream caused a drag increment due to friction. It can be concluded that in general longer ranges lead to a higher PREE, especially for those aircraft with a secondary powertrain when take-off and landing are not limiting constraints. The beneficial aero-propulsive effects can act over a longer duration to overcome their mass penalties. Additionally, DHEP can be beneficial in low speed applications in case take-off distance or landing are constraining the design. At the long-range case for Mach 0.5, the distributed propulsion systems show the largest improvement. Overall, the DHEP aircraft (in their unoptimized form) seem to perform similar as their reference cases. As the references are well understood, their inputs are more optimal and, as shown in other works, the cruise altitude has a significant impact on the performance of DHEP aircraft. Therefore, future investigations with relatively low shaft power ratios, and even medium technology scenarios should focus on more optimal layout for DHEP aircraft concepts to target improvements in terms of PREE, at the cost of some MTOM penalty.

More detailed investigations are required into the installation effects of distributed (wing-mounted) propulsion, incorporating both aero-elastic effects as well as the effects of propeller installation angle with respect to the main wing. At present, this is a limitation of the LLM model that was implemented for these studies, leading to a likely underprediction of the increments in lift coefficient due to the distributed leading-edge propellers. The current LLM surrogate model is conservative, when compared to e.g. the deltas computed in Ref.[27] Additionally, noise aspects should be considered in the conceptual aircraft design, which also calls for an investigation of ducted propellers and their performance. Duct design can be critical in terms of propeller performance as well as incurred mass penalty. The conceptual design should also include to-be-developed methods for low-speed high-lift conditions of distributed (wing-mounted) propulsion, including their effect on pitching moment. This is also key to allow the necessary inclusion of stability and control assessments (directional, lateral and longitudinal). A further investigation of the wing mass penalty associated with additional pylons and mounting points (secondary structure) is required, as the sizing of these components is currently based on empirical methods.

Acknowledgments

This work was partially funded by the European Union Horizon 2020 program, as part of the Clean Sky 2 program, Large Passenger Aircraft (CS2-LPA-GAM-2018-2019-01). The authors would like to thank all Clean Sky 2 WP1.6.1.4

partners for their feedback, discussions and technical insight. Furthermore, we would like to thank Nando van Arnhem, Tom Stokkermans, Biagio Della Corte, Martijn van Sluis, Peijian Lv, Tarik Hartuc and Leo Veldhuis (all Delft University of Technology) for their contributions to the used aero-propulsive models, as well as Reno Elmendorp and Martijn Roelofs (also Delft University of Technology) for their developments of the Class-II.5 weight estimations.

References

[1] Anonymous, "Flightpath 2050: Europe's Vision for Aviation. Report of the High Level Group on Aviation Research," , 2011.

[2] Felder, J. L., "NASA electric propulsion system studies," 2015.

[3] Borer, N. K., Patterson, M. D., Viken, J. K., Moore, M. D., Clarke, S., Redifer, M. E., Christie, R. J., Stoll, A. M., Dubois, A., Bevirt, J. B., Gibson, A. R., Foster, T. J., and Osterkamp, P. G., "Design and Performance of the NASA SCEPTOR Distributed Electric Propulsion Flight Demonstrator," *16th AIAA Aviation Technology, Integration, and Operations Conference, Washington, DC, USA*, American Institute of Aeronautics and Astronautics, American Institute of Aeronautics and Astronautics, 2016. doi:10.2514/6.2016-3920.

[4] Antcliff, K. R., and Capristan, F. M., "Conceptual Design of the Parallel Electric-Gas Architecture with Synergistic Utilization Scheme (PEGASUS) Concept," *18th AIAA/ISSMO Multidisciplinary Analysis and Optimization Conference, Denver, Colorado, USA*, American Institute of Aeronautics and Astronautics, American Institute of Aeronautics and Astronautics, 2017. doi:10.2514/6.2017-4001.

[5] Rothhaar, P. M., Murphy, P. C., Bacon, B. J., Gregory, I. M., Grauer, J. A., Busan, R. C., and Croom, M. A., "NASA langley distributed propulsion VTOL tilt-wing aircraft testing, modeling, simulation, control, and flight test development," *Proceedings of the 14th AIAA Aviation Technology, Integration, and Operations Conference, Atlanta, GA, USA*, American Institute of Aeronautics and Astronautics, American Institute of Aeronautics and Astronautics, 2014. doi:10.2514/6.2014-2999.

[6] Schiltgen, B. T., and Freeman, J., "Aeropropulsive interaction and thermal system integration within the ECO-150: a turboelectric distributed propulsion airliner with conventional electric machines," *16th AIAA Aviation Technology, Integration, and Operations Conference, Washington, DC, USA*, American Institute of Aeronautics and Astronautics, 2016. doi:10.2514/6.2016-4064.

[7] Hermetz, J., Ridel, M., and Döll, C., "Distributed electric propulsion for small business aircraft: A concept-plane for key-technologies investigations," *Proceedings of the 30th Congress of the International Council of the Aeronautical Sciences, Daejeon, South Korea*, International Council of the Aeronautical Sciences, 2016.

[8] Stoll, A. M., and Mikić, G. V., "Design Studies of Thin-Haul Commuter Aircraft with Distributed Electric Propulsion," *16th AIAA Aviation Technology, Integration and Operations Conference, Washington, DC, USA*, American Institute of Aeronautics and Astronautics, American Institute of Aeronautics and Astronautics, 2016. doi:10.2514/6.2016-3765.

[9] Jansen, R. H., Bowman, C., Jankovsky, A., Dyson, R., and Felder, J., "Overview of NASA Electrified Aircraft Propulsion Research for Large Subsonic Transports," *53rd AIAA/SAE/ASEE Joint Propulsion Conference, Atlanta, GA, USA*, American Institute of Aeronautics and Astronautics, American Institute of Aeronautics and Astronautics, 2017. doi:10.2514/6.2017-4701.

[10] Sgueglia, A., Schmollgruber, P., Bartoli, N., Atinault, O., Benard, E., and Morlier, J., "Exploration and Sizing of a Large Passenger Aircraft with Distributed Ducted Electric Fans," *2018 AIAA Aerospace Sciences Meeting*, American Institute of Aeronautics and Astronautics, 2018. doi:10.2514/6.2018-1745.

[11] Steiner, H. J., Seitz, A., Wieczorek, K., Plötner, K., Iskiveren, A. T., and Hornung, M., "Multi-disciplinary design and feasibility study of distributed propulsion systems," *Proceedings of the 28th ICAS Congress, Brisbane, Australia*, International Council of the Aeronautical Sciences, 2012.

[12] Voskuijl, M., van Bogaert, J., and Rao, A. G., "Analysis and design of hybrid electric regional turboprop aircraft," *CEAS Aeronautical Journal*, Vol. 9, No. 1, 2018, pp. 15–25.

[13] de Vries, R., Hoogreef, M. F. M., and Vos, R., "Preliminary Sizing of a Hybrid-Electric Passenger Aircraft Featuring Over-the-Wing Distributed-Propulsion," *AIAA Scitech 2019 Forum*, American Institute of Aeronautics and Astronautics, 2019. doi:10.2514/6.2019-1811.

[14] Hoogreef, M. F. M., Vos, R., de Vries, R., and Veldhuis, L. L. M., "Conceptual Assessment of Hybrid Electric Aircraft with Distributed Propulsion and Boosted Turbofans," *AIAA Scitech 2019 Forum*, American Institute of Aeronautics and Astronautics, 2019. doi:10.2514/6.2019-1807.

[15] Zamboni, J., Vos, R., Emeneth, M., and Schneegans, A., "A method for the conceptual design of hybrid electric aircraft," *AIAA Scitech 2019 Forum*, American Institute of Aeronautics and Astronautics, 2019. doi:10.2514/6.2019-1587.

[16] Veldhuis, L. L. M., "Propeller wing aerodynamic interference," Dissertation, Delft University of Technology, July 2005. ISBN: 90-9019537-8.

[17] de Vries, R., Brown, M. T., and Vos, R., "A Preliminary Sizing Method for Hybrid-Electric Aircraft Including Aero-Propulsive Interaction Effects," *2018 Aviation Technology, Integration, and Operations Conference*, American Institute of Aeronautics and Astronautics, 2018. doi:10.2514/6.2018-4228.

[18] Marcus, E. A., de Vries, R., Kulkarni, A. R., and Veldhuis, L. L. M., "Aerodynamic Investigation of an Over-the-Wing Propeller for Distributed Propulsion," *2018 AIAA Aerospace Sciences Meeting*, American Institute of Aeronautics and Astronautics, 2018. doi:10.2514/6.2018-2053.

[19] Stokkermans, T. C. A., van Arnhem, N., Sinnige, T., and Veldhuis, L. L. M., "Validation and Comparison of RANS Propeller Modeling Methods for Tip-Mounted Applications," *AIAA Journal*, Vol. 57, No. 2, 2019, pp. 566–580. doi:10.2514/1.J057398.

[20] Sinnige, T., van Arnhem, N., Stokkermans, T. C. A., Eitelberg, G., and Veldhuis, L. L. M., "Wingtip-Mounted Propellers: Aerodynamic Analysis of Interaction Effects and Comparison with Conventional Layout," *Journal of Aircraft*, Vol. 56, No. 1, 2018, pp. 295–312. doi:10.2514/1.c034978.

[21] van Arnhem, N., Sinnige, T., Stokkermans, T. C. A., Eitelberg, G., and Veldhuis, L. L. M., "Aerodynamic Interaction Effects of Tip-Mounted Propellers Installed on the Horizontal Tailplane," *2018 AIAA Aerospace Sciences Meeting*, American Institute of Aeronautics and Astronautics, 2018. doi:10.2514/6.2018-2052.

[22] van Arnhem, N., Vos, R., and Veldhuis, L. L. M., "Aerodynamic Loads on an Aft-Mounted Propeller Induced by the Wing Wake," *AIAA Scitech 2019 Forum*, American Institute of Aeronautics and Astronautics, 2019. doi:10.2514/6.2019-3036.

[23] Harinarain, V., "Aerodynamic Performance Study on Ducted Propeller System for Propulsion and Control and Stability Applications," Master's thesis, 2017.

[24] Lv, P., Rao, A. G., Ragni, D., and Veldhuis, L. L. M., "Performance Analysis of Wake and Boundary-Layer Ingestion for Aircraft Design," *Journal of Aircraft*, Vol. 53, No. 5, 2017, pp. 1517–1526. doi:10.2514/1.c033395.

[25] Lv, P., Ragni, D., Hartuc, T., Veldhuis, L. L. M., and Rao, A. G., "Experimental investigation of the flow mechanisms associated with a wake-ingesting propulsor," *AIAA Journal*, Vol. 55, No. 4, 2017, pp. 1332–1342. doi:10.2514/1.j055292.

[26] Vos, R., and Hoogreef, M. F. M., "System-level assessment of tail-mounted propellers for regional aircraft," *Proceedings of the 31st Congress of the International Council of Aeronautical Sciences*, 2018.

[27] de Vries, R., Brown, M., and Vos, R., "Preliminary Sizing Method for Hybrid-Electric Distributed-Propulsion Aircraft," *Journal of Aircraft*, Vol. 56, No. 6, 2019, pp. 1–17. doi:10.2514/1.c035388.

[28] de Vries, R., Hoogreef, M. F. M., and Vos, R., "Aeropropulsive Efficiency Requirements for Turboelectric Transport Aircraft," *AIAA Scitech 2020 Forum*, 2020.

[29] Elmendorp, R. J. M., Vos, R., and La Rocca, G., "A conceptual design and analysis method for conventional and unconventional airplanes," *ICAS 2014: Proceedings of the 29th Congress of the International Council of the Aeronautical Sciences, St. Petersburg, Russia, 7-12 September 2014*, International Council of Aeronautical Sciences, 2014.

[30] Schut, J., and van Tooren, M. J. L., "Design" Feasilization" Using Knowledge-Based Engineering and Optimization Techniques," *Journal of Aircraft*, Vol. 44, No. 6, 2007, pp. 1776–1786. doi:10.2514/1.24688.

[31] Vos, R., and Hoogreef, M. F. M., "Semi-analytical weight estimation method for fuselages with oval cross-section," *54th AIAA/ASME/ASCE/AHS/ASC Structures, Structural Dynamics, and Materials Conference*, American Institute of Aeronautics and Astronautics, 2013. doi:10.2514/6.2013-1719.

[32] Schmidt, K., and Vos, R., "A semi-analytical weight estimation method for oval fuselages in conventional and novel aircraft," *52nd Aerospace Sciences Meeting*, American Institute of Aeronautics and Astronautics, 2014. doi:10.2514/6.2014-0026.

[33] Roelofs, M., and Vos, R., "Semi-analytical composite oval fuselage weight estimation," *55th AIAA Aerospace Sciences Meeting*, American Institute of Aeronautics and Astronautics, 2017. doi:10.2514/6.2017-0466.

[34] Elmendorp, R. J. M., and La Rocca, G., "Comparitive Design & Sensitivity Studies on Box-Wing Airplanes," *Italian Association of Aeronautics and Astronautics - XXV International Congress*, 2019.

[35] Finger, D. F., Braun, C., and Bil, C., "An initial sizing methodology for hybrid-electric light aircraft," *2018 Aviation Technology, Integration, and Operations Conference*, American Institute of Aeronautics and Astronautics, 2018. doi:10.2514/6.2018-4229.

[36] Finger, D. F., de Vries, R., Braun, C., Vos, R., and Bil, C., "A Comparison of Hybrid-Electric Aircraft Sizing Methods," *AIAA Scitech 2020 Forum*, 2020.

[37] Anonymous, *Commercial aircraft propulsion and energy systems research: reducing global carbon emissions*, National Academies Press, 2016. National Academies of Sciences, Engineering, and Medicine; Division on Engineering and Physical Sciences; Aeronautics and Space Engineering Board; Committee on Propulsion and Energy Systems to Reduce Commercial Aviation Carbon Emissions.

[38] Stückl, S., "Methods for the Design and Evaluation of Future Aircraft Concepts Utilizing Electric Propulsion Systems," Ph.D. thesis, Technische Universität München, 2016.

[39] Ting, L., and Liu, C. H., "Thin Airfoil in Nonuniform Parallel Stream," *Journal of Aircraft*, Vol. 6, No. 2, 1969, pp. 173–175. doi:10.2514/3.44030.

[40] Ting, L., Liu, C. H., and Kleinstein, G., "Interference of Wing and Multipropellers," *AIAA Journal*, Vol. 10, No. 7, 1972, pp. 906–914. doi:10.2514/3.50244.

[41] Torenbeek, E., *Synthesis of subsonic airplane design*, Delft University Press, 1982.

[42] Habermann, A. L., Bijewitz, J., Seitz, A., and Hornung, M., "Performance Bookkeeping for Aircraft Configurations with Fuselage Wake-Filling Propulsion Integration," *Deutscher Luft- und Raumfahrtkongress (DLRK) 2018*, 46 September 2018.

[43] Smith Jr., L. H., "Wake Ingestion Propulsion Benefit," *Journal of Propulsion and Power*, Vol. 9 (No. 1), No. 1, 1993, pp. 74–83. doi:10.2514/3.11487.

[44] Mikić, G. V., Stoll, A. M., Bevirt, J., Grah, R., and Moore, M. D., "Fuselage Boundary Layer Ingestion Propulsion Applied to a Thin Haul Commuter Aircraft for Optimal Efficiency," *16th AIAA Aviation Technology, Integration, and Operations Conference*, American Institute of Aeronautics and Astronautics, 2016. doi:10.2514/6.2016-3764.

[45] ESDU, "The influence of body geometry and flow conditions on axisymmetric velocity distributions at subcritical Mach numbers," ESDU 78037, 1978.

[46] ESDU, "The influence of body geometry and flow conditions on axisymmetric boundary layers at subcritical Mach numbers," ESDU 79020, 1979.

[47] Seitz, A., Peter, F., Bijewitz, J., Habermann, A., Goraj, Z., Kowalski, M., Castillo, A., Meller, F., Merkler, R., Samuelsson, S., et al., "Concept Validation Study for Fuselage Wake-Filling Propulsion Integration," *31st Congress of the International Council of the Aeronautical Sciences*, 2018, pp. 09–14.

[48] Schouten, T., Hoogreef, M. F. M., and Vos, R., "Effect of Propeller Installation on Performance Indicators of Regional Turboprop Aircraft," *AIAA Scitech 2019 Forum*, American Institute of Aeronautics and Astronautics, 2019. doi:10.2514/6.2019-1306.

[49] Bijewitz, J., Seitz, A., Isikveren, A. T., and Hornung, M., "Progress in optimizing the propulsive fuselage aircraft concept," *54th AIAA Aerospace Sciences Meeting*, American Institute of Aeronautics and Astronautics, 2016. doi:10.2514/6.2016-0767.